

Influence of urea on electrocatalytic oxidation of ethylene glycol on porous CuOx/Cu foam anode in alkaline medium

Aya M. Saada^{1,2}, Mohamed A. Sadek³, Mohamed E. El-Shakre¹, Ahmed A. El-Sherif^{1,*}

¹ Department of Chemistry, Faculty of Science, Cairo University, Cairo, Egypt.

² Department of Biochemical Engineering, Faculty of Energy and Environmental Engineering, The British University in Egypt (BUE), El-Shorouk, Cairo 11837, Egypt.

³ Department of Chemical Engineering, Faculty of Engineering, The British University in Egypt (BUE), El-Shorouk, Cairo 11837, Egypt.

*E-mail: shahir.sadek@bue.edu.eg, elshakre@sci.cu.edu.eg, aelsherif@sci.cu.edu.eg

Received: 17 June 2022 / Accepted: 11 August 2022 / Published: 10 September 2022

This study addresses the enhanced electrocatalytic oxidation of ethylene glycol (EG) at Cu oxide (CuOx) microporous catalyst in alkaline medium. A foam-like microporous CuOx film is successfully electrodeposited using the dynamic hydrogen bubble template (DHBT) technique. The structural and morphological characterizations of the microporous film are carried out by XRD and SEM techniques, respectively. The influence of urea (as a blending fuel) on the electro-oxidation of EG is investigated by cyclic voltammetry (CV), linear sweep voltammetry (LSV), electrochemical impedance spectroscopy (EIS), and chronoamperometry (*i-t*) measurements. The oxidation peak current of EG is improved by addition of urea with a concurrent favorable negative shift of the onset potential of the oxidation process. A plausible model in which the formation of a linear chain and/or a 9-membered ring structures is proposed between urea and EG (via hydrogen bonding) with a favorable total lower energy and enhanced dipole moment (as evident from DFT calculations). This geometry enhances the proper adsorption orientation of EG on the electrode surface and thus facilitates its oxidation.

Keywords: Fuel cells, Energy conversion, Porous catalysts, Non-Pt catalysts, DFT calculations.

1. INTRODUCTION

The global concern about decarbonization together with the growing world population and the unlimited needs for energy call for the development of renewable and sustainable energy production routes [1-5]. Among the most promising systems, fuel cells (FCs) technology is rapidly developing to meet these energy requirements. In view of their virtues, FCs are unique entry into the era of quiet, noiseless and eco-friendly electric power generating devices [6,7]. Among the different types of FCs, alkaline FCs are progressively developing [8] and extensively studied during the last four decades. In this context, polymer electrolyte membrane (PEM) FCs emerged as a new technology with higher

flexibility while using solid electrolyte to avoid the electrolyte leakage. Among which, alkaline direct alcohol FCs open up the avenue for low-cost metal catalyst, e.g., Ag, Ni, and Pd [9-14]. Methanol as well as ethanol and ethylene glycol (EG) are promising low molecular weight candidates for use as fuels [15-17]. In this context, the significant hydrogen content and the liquid nature of EG (HO-CH₂-CH₂-OH) in addition to its high energy density render it a suitable fuel for energy conversion systems. For instance, direct EGFCs have a volumetric energy density of 5.90 kWhL⁻¹, which outweighs direct methanol FCs (DMFCs, 4.69 kWhL⁻¹) and direct formic acid FCs (2.09 kWhL⁻¹) [18-21]. Moreover, and advantageously, EG is less toxic, less volatile (B.P = 197.3°C) which allows for high temperature operation of the PEMFC, thus, facilitate the C-C bond breakage (towards the complete oxidation to CO₂ via a 10-electron process) [22-26]. In view of this virtues, EG oxidation has been extensively studied at several anodes with an aim to minimize the charge transfer resistance (during the oxidation process), on the one hand, and to reduce the cost of the anode components, on the other hand, while maintaining a prolonged activity. This includes the use of metal and/or metal oxide composites [21,25-33].

In this study, a porous foam-like film of CuOx/Cu is prepared using the dynamic hydrogen bubbles technique (DHBT) and its electrocatalytic activity towards EG oxidation is investigated in alkaline medium. The morphology and the crystal structure of the as-prepared foam-like porous film is probed by SEM and XRD techniques, respectively. The prepared film shows good electrocatalytic activity towards EG oxidation compared with the corresponding planar electrode as depicted from CV measurements. The influence of urea, as an additive (i.e., a blending fuel), on EG oxidation is investigated as well, with enhancement factor depending on the molar ratio of urea. DFT calculations supported a proposed model which is introduced to interpret the observed behavior; where two important quantum chemical parameters, i.e., the total energy and the dipole moments (of the binary fuel blend) are calculated and correlated with the observed enhancement.

2. EXPERIMENTAL

2.1. Electrodes and Chemicals

The working electrode is a Cu rod (4.0 mm in-diameter) mounted in a glass tube with epoxy resin leaving a geometric surface area of 0.125 cm². The reference and the counter electrodes are Ag/AgCl/KCl(sat.) and graphite rod, respectively. The working electrode is mechanically polished by successively higher grits emery papers (up to 3000) to a mirror finish, and then rinsed with distilled water. The electrodeposition of the foam-like Cu microporous film on the cleaned Cu (CuOx/Cu) electrode is achieved by applying a constant potential electrolysis of -2.5 V vs. Ag/AgCl/KCl(sat) in an aqueous solution of 0.5 M H₂SO₄ containing 0.1 M CuSO₄ allowing the passage of 3 Coulombs, leading to the deposition of 418 µg. This step is followed with electrochemical passivation of the foam-like Cu film to form Cu oxide by cycling the potential 3 times between -1.5 V to 0.9 V vs. Ag/AgCl/KCl(sat) in 0.5 M NaOH (*c.f.* Fig. 4). The as prepared catalyst layer will be referred hereafter as CuOx/Cu foam. All chemicals used in this study were of analytical grade, purchased from Sigma Aldrich (Germany) and were used without further purification. All solutions were freshly prepared using distilled water.

2.2. Surface and electrochemical characterization

The morphology and the crystal structure of the as-prepared CuOx/Cu foam were probed by field emission scanning electron microscope (FE-SEM, QUANTA FEG250) and X-ray diffraction spectrometer, XRD (PANalytical, X'Pert PRO). All electrochemical experiments were carried out using a Bio-Logic potentiostat (Model VSP-300) at ambient temperature ($25 \pm 1^\circ\text{C}$). The electrocatalytic activity of the as-prepared foam-like CuOx working electrode towards ethylene glycol oxidation were carried out using a three-electrode cell in 0.5 M NaOH containing 0.1 M ethylene glycol. Controlled amounts of urea were added to this solution to investigate its impact on the electro-oxidation of ethylene glycol. This is done by measuring the cyclic voltammetry (CV), linear sweep voltammetry (LSV), electrochemical impedance spectroscopy (EIS) and responses and chronoamperometry ($i-t$ curves) under several operating conditions.

3. RESULTS AND DISCUSSION

3.1. Morphological, structure and electrochemical characterization:

Fig. 1 shows SEM image of the thus-prepared CuOx/Cu foam. This figure indicates the formation of a 3-D porous open structure atop the Cu substrate. The porosity of the Cu film is induced by the simultaneous evolution of hydrogen gas (acting as a dynamic template) during the Cu electrodeposition.

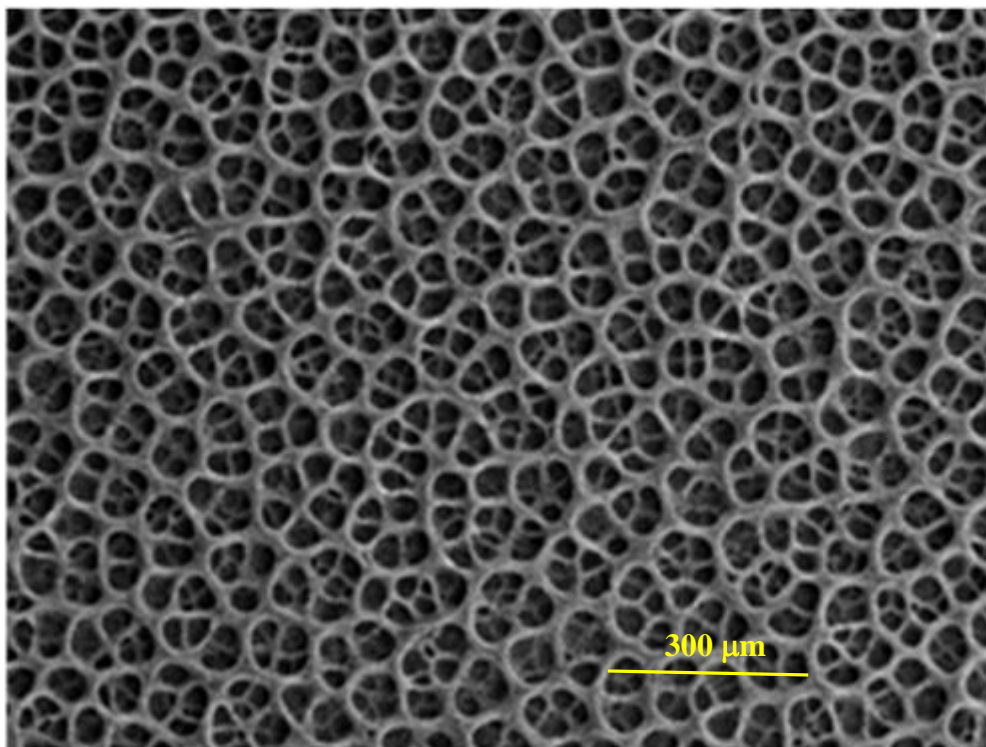


Figure 1. SEM image of the porous CuOx/Cu foam-like film.

The highly open structure of CuOx/Cu foam is characterized by a high roughness and thus a high real surface area. This is probed by measuring the redox CV response of potassium ferricyanide (1 M KCl + 5 mM $K_4[Fe(CN)_6]$) at the bare Cu substrate and the porous catalyst layer, as shown in Fig. 2. This figure indicates that the porous Cu foam-like catalyst has a surface area of ca. 3 times that of the bare Cu. Fig. 3 shows XRD pattern of the thus-prepared CuOx/Cu foam. The crystallinity of the porous film is verified by the sharp peaks located at 2θ of ca. 44° , 51° , and 74° , corresponding to the (111), (200) and (220) FCC planes of metallic Cu, respectively, (COD 4313211) whereas, the diffraction peaks located at 2θ of ca. 36° , 42° and 61° refer to the FCC crystal structure of copper oxide (Cu_2O), (COD 1000063).

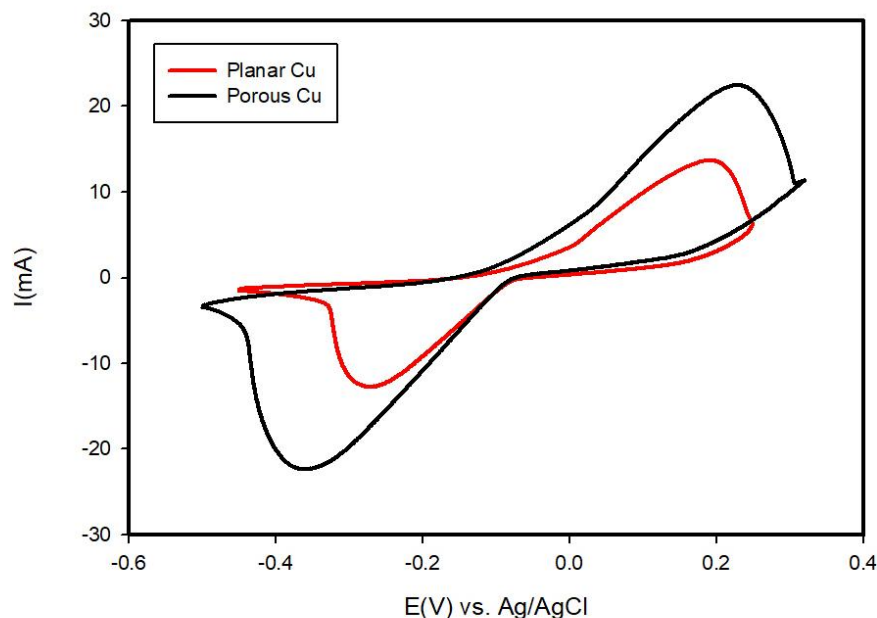


Figure 2. CV response of 5.0 mM $K_4[Fe(CN)_6]$ + 1.0 M KCl at 100 mV s^{-1} obtained at (a) bare Cu and (b) Cu foam-like porous catalyst.

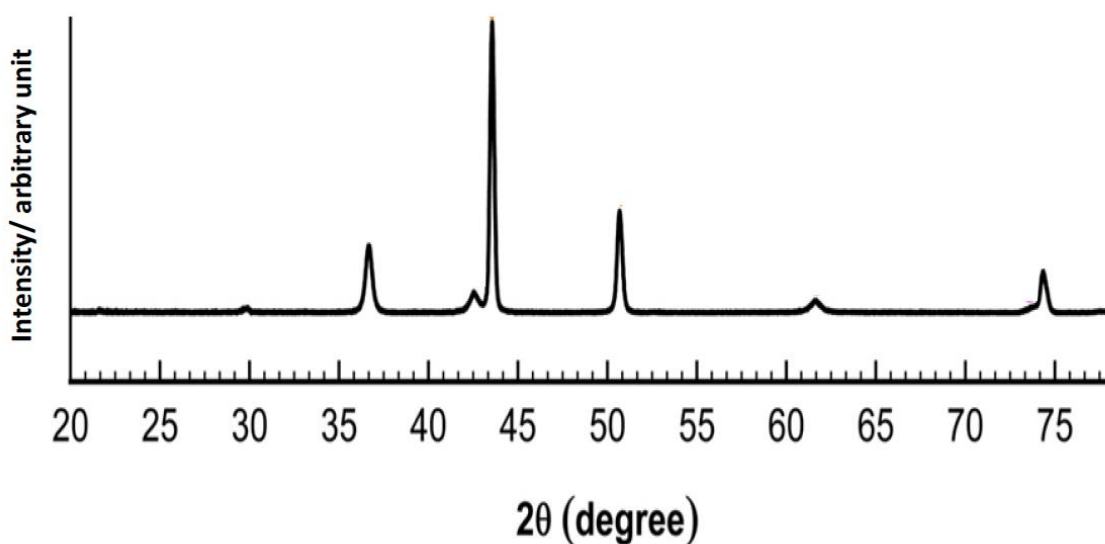


Figure 3. XRD pattern of the as-prepared Cu foam-like porous catalyst.

Fig. 4 shows the CV response of bare Cu substrate and the porous CuOx/Cu foam-like catalyst measured in 0.5 M NaOH. The presence of several redox peaks, within the employed potential window, indicates the variation of the copper oxidation states as a function of potential. For instance, the oxidation peaks observed at -0.5 V and 0.0 V are assigned to the transformation of metallic Cu to Cu₂O and CuO/Cu(OH)₂, respectively [34-36]. Meanwhile, during the negative-going potential scan, the high oxidation states of Cu²⁺ and Cu⁺ are reduced back to metallic copper. Noteworthy to mention here that the intensity of the redox peaks obtained at the porous catalyst layer is much higher than those obtained at the bare Cu, reflecting a marked difference in the active surface area [37-39], consistently with the CV response obtained for the ferricyanide redox (Fig. 2).

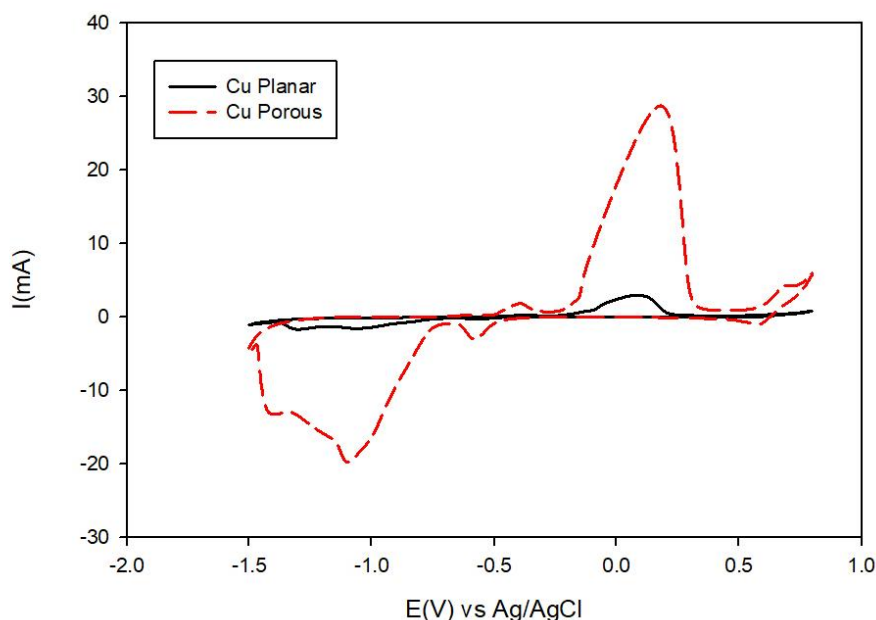
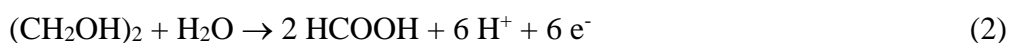


Figure 4. CVs measured at planar Cu (black solid line) and porous CuOx/Cu foam-like catalyst (red dashed line) in 0.5 M NaOH. Potential scan rate = 50 mV s⁻¹.

3.2. Ethylene glycol electro-oxidation

Fig. 5 shows the CV response of ethylene glycol electro-oxidation obtained at CuOx/Cu foam catalyst measured in 0.5 M NaOH containing 0.1 M ethylene glycol. A blank CV is measured in ethylene glycol-free NaOH (dashed curve). This figure reflects the ability of the Cu oxide/Cu foam-like porous catalyst to oxidize EG without the need of precious metals (e.g., Pt) as evident by the observation of oxidation peak at ca. 0.7 V and the oxidation commences at onset potential of ca. 0.4 V. It is worth mentioning here that oxalic acid and formic acid are possible oxidation products of EG, based on HPLC analysis [25,40-42] according to:



Subsequently, the electro-oxidation of formic acid to CO₂ proceeds according to:



Also, the oxidation peak current increases by the increase of EG concentration and/or increase of the potential scan rate. The origin of the catalytic activity of CuO_x/Cu foam catalyst might be attributed to a mediated catalytic activity of Cu ions in various oxidation states [43-47] including the redox transformation between copper oxides/hydroxides, e.g.:



Thus, the produced CuOOH (with high oxidizing power) acts as a catalytic mediator for EG as follows:

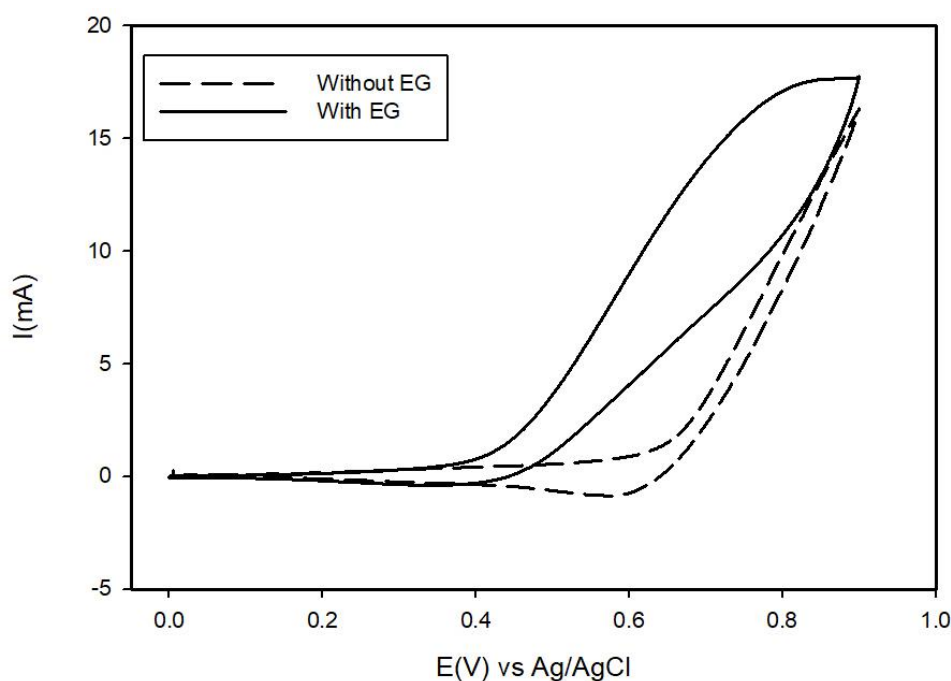
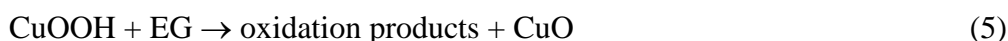


Figure 5. CV response measured at CuO_x/Cu foam-like porous catalyst in 0.5 M NaOH without (dashed line) and with 0.1 M ethylene glycol (solid line). Potential scan rate = 50 mV s⁻¹.

3.3. Impact of urea as a blending fuel:

Fig. 6 shows the LSV response for EG electro-oxidation measured at the porous CuO_x/Cu foam-like catalyst in 0.5 M NaOH containing 0.1 M EG with various amounts of urea. Inspection of this figure reveals that the presence of urea (as an additive) enhances the oxidation current of EG to various extents (depending on the molar ratio of the additive), concurrently with a favorable negative shift of the onset potential of EG oxidation. That is the addition of minute amount of urea (0.005 M) to EG (0.1M) resulted

in an increase of the oxidation current from 16.3 mA to 17.7 mA, in the absence and the presence of urea, respectively, together with a favorable negative shift of the onset potential by ca. 100 mV.

The enhancement factor ($EF = I_{p(\text{in presence of urea})}/I_{p(\text{in absence of urea})}$) of the oxidation peak current is plotted vs. the mole fraction of urea (X_{urea}), shown in Fig. 7. This figure indicates that EF increases with X_{urea} , reaching a peak value at $X_{\text{urea}} = 0.17$, after which EF declines and reaches a plateau value of ca. 1.1 at $X_{\text{urea}} \geq 0.36$.

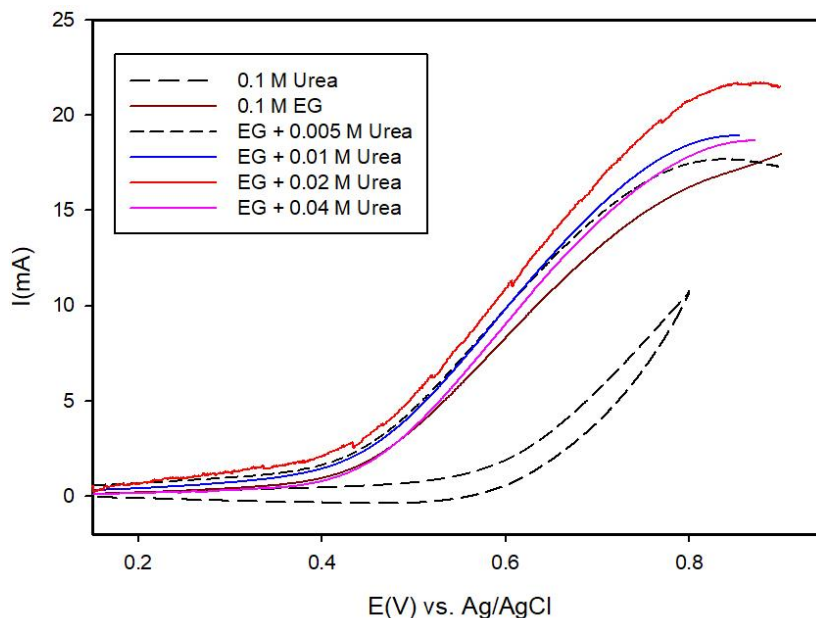


Figure 6. LSV response measured for EG oxidation at CuOx/Cu foam-like porous catalyst in 0.5 M NaOH + 0.1 M EG in the presence of various amounts of urea. Potential scan rate = 50 mV s⁻¹.

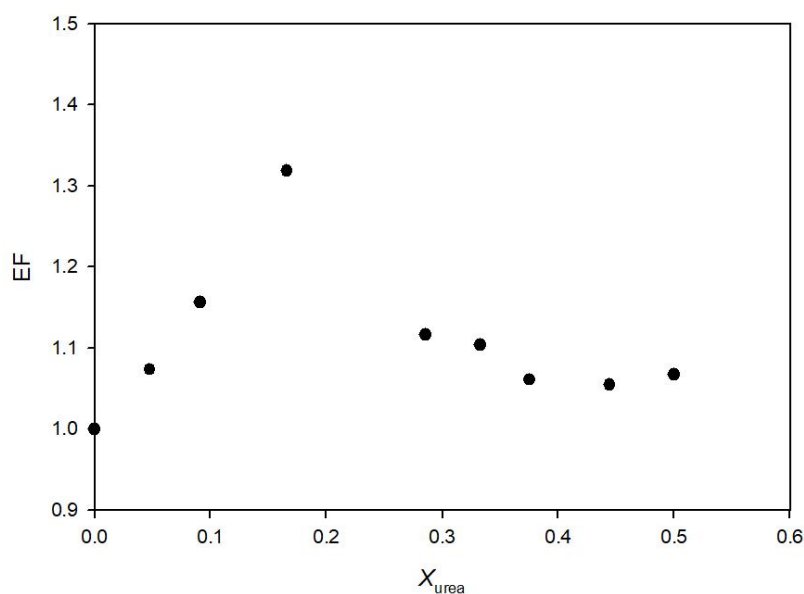


Figure 7. Variation of the enhancement factor ($EF = I_{p(\text{in presence of urea})}/I_{p(\text{in absence of urea})}$) for EG oxidation current vs. urea mole fraction (X_{urea}).

Moreover, electrochemical impedance spectroscopy (EIS) is measured to probe the influence of the addition of urea on the charge transfer resistance during ethylene glycol oxidation as shown in Fig. 8. This figure displays the Nyquist plots of ethylene glycol electro-oxidation at CuO_x/Cu porous foam-like anodes in 0.5 M NaOH + 0.1 M EG in the absence (solid line) and the presence of 0.02 M urea (dotted line) measured at 0.35 V. Nyquist plots (displayed in semi-circles) are attributed to kinetically controlled process at higher frequencies [48]. The impedance parameters are calculated by fitting the experimentally measured EIS data using the Randles equivalent circuit model. The diameter of each semi-circle represents the charge transfer resistance (R_{CT}), which amounts to 186.36 ohms and 134.84 ohms, in the absence and the presence of urea, respectively. The lowering of R_{CT} in the presence of urea provides further evidence for its enhancing role during EG oxidation.

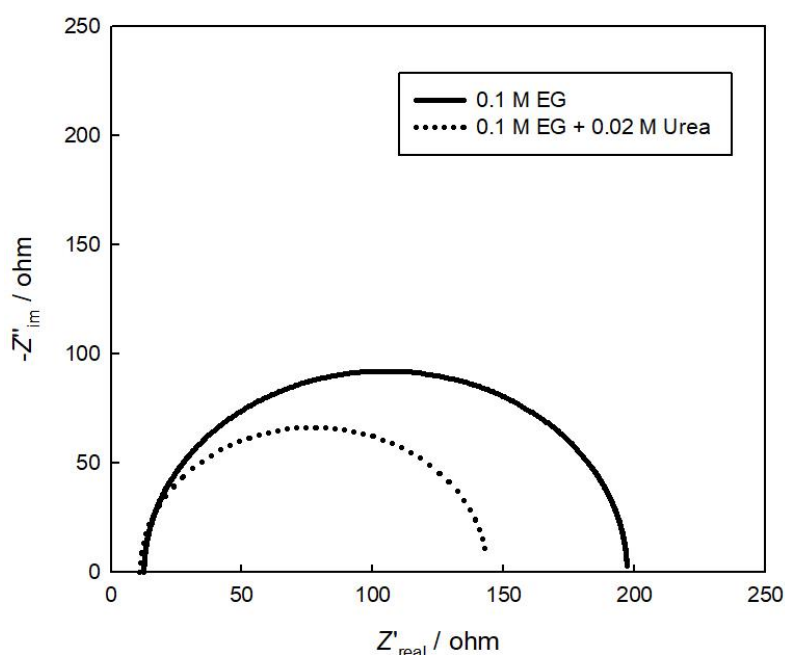


Figure 8. Nyquist plots of ethylene glycol electro-oxidation at CuO_x/Cu porous foam-like anodes in 0.5 M NaOH + 0.1 M EG in the absence (solid line) and the presence of 0.02 M urea (dotted line) measured at 0.35 V vs. Ag/AgCl/KCl(sat).

The stability of the electrocatalysts has long been probed by measuring either potential-time ($E-t$) correlations at fixed current density or current-time ($i-t$) correlations at a fixed operating potential [49-51]. In the current study the stability of the proposed CuO_x/Cu porous foam-like catalyst is probed by measuring the $i-t$ curves for EG oxidation recorded at 0.65 V vs. Ag/AgCl/KCl(sat) in (a) absence and (b) presence of urea (Fig. 9). This figure shows that the presence of urea (curve b) supports a higher oxidation current of EG for a prolonged electrolysis time. The enhancing role of urea could be reasonably attributed to a favorable geometric interaction with EG via H-bonding, thus, forming a linear binary chain of EG-urea and/or a 9-membered ring as described in Table 1 (given below). This favorable

structural geometry is thought to stabilize EG in the vicinity of the electrode and allows its facile oxidation as supported by the relevant DFT calculations.

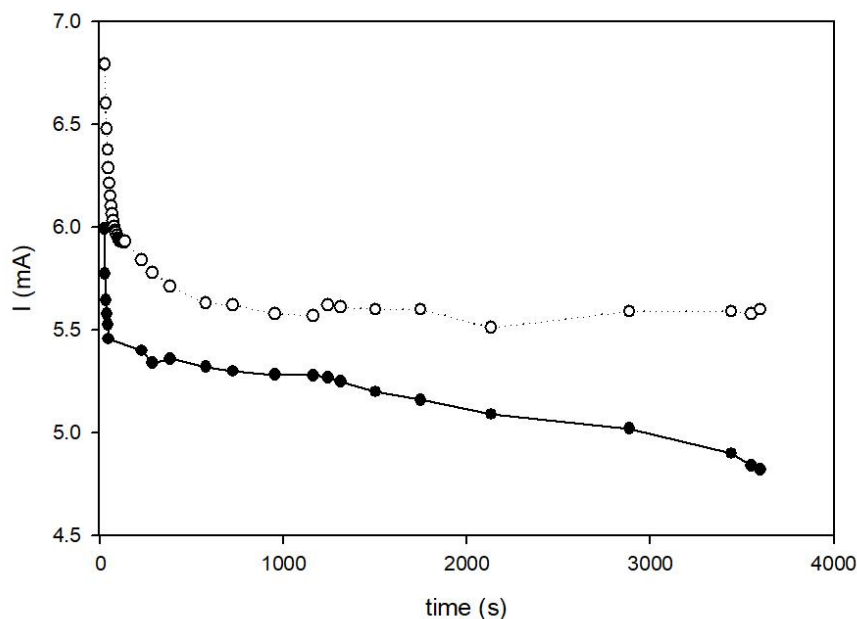


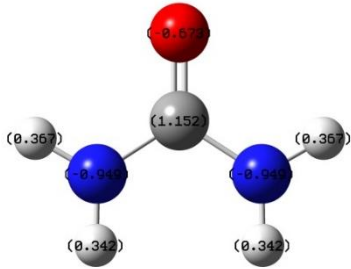
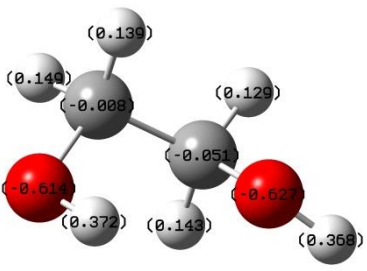
Figure 9. *i-t* curves for EG electro-oxidation recorded at 0.65 V vs. Ag/AgCl/KCl(sat) measured at CuO_x/Cu porous foam-like anodes in 0.5 M NaOH + 0.1 M EG in the absence (solid line, black symbols) and the presence of urea (dashed line, open symbols, $X_{\text{urea}} = 0.17$).

3.4. DFT calculations:

Blending of two small organic molecules has shown a synergistic enhancement towards the electro-oxidation at nanoparticle-based electrocatalysts [52-55]. For instance formic acid oxidation has been enhanced upon blending with either methanol or urea [52, 55]. In this context, urea has been suggested as a blending fuel to boost the electro-oxidation of formic acid and ascorbic acid at nanoparticle-based anodes [54,55], where urea acted as anchoring antennae for the small organic molecule in such a way that facilitates its oxidation pathway. DFT calculations were taken as a probing criterion to support this assumption. Two important quantum chemical parameters were evaluated, i.e., the total energy of the individual molecules vs. the binary structure of the urea-blended with the target fuel and the dipole moment as well [54-56]. A plausible model is proposed assuming the formation of urea-ethylene glycol chain-like geometry via H-bonding with a favorable lower energy that stabilizes ethylene glycol in the vicinity of the anode thus facilitates its oxidation. The depicted geometry is obtained by computational calculations using Gaussian 09 software, and applying density functional theory (DFT) using B3LYP method/Basis Set = 6-311G (the obtained results are listed in Table 1. This table shows the charge distribution at each atom where, N atom of urea carries the highest negative charge (-0.949) compared with the oxygen atom (-0.673) in urea. Thus, N atom in urea is the most probable binding site for H-bonding with ethylene glycol. On the other hand, the calculated charges on the oxygen atoms in ethylene glycol are -0.614 and -0.627. This implies that the H-bonding between urea and ethylene glycol takes place via the H (carrying charges of +0.372 and +0.368) of the two OH

groups in ethylene glycol and the two terminal N atoms in urea. Inspection of this table reveals that the formed binary fuel has a total lower energy compared with the individual compounds, indicating its feasible formation and the improved dipole moment forced the binary urea-EG blend to approach the polarized electrode (anode) surface in a favorable orientation that facilitates the further oxidation of EG. Thus, the double layer in the electrode vicinity enriched with the highly polar urea-EG blend, leading to possible acceleration of the electro-oxidation reaction rate. In this way, urea is believed to act as antennae (carrier) to capture EG from the bulk electrode to the electrode surface enabling its oxidation. A similar enhancing role of urea towards the electro-oxidation of formic acid has been investigated on Pd-based electrocatalysts [54,55]. However, the advantage of the current study is the use of non-precious metal (i.e., Cu) as the sole catalyst. Further investigations are underway to clarify the blending effect of urea on the electro-oxidation of other low molecular weight organic compounds at non-precious metal-based electrocatalysts.

Table 1. Optimized structures and geometries of urea, ethylene glycol (EG) and urea-EG binary systems with the corresponding calculated total energy (a.u.) and dipole moments (Debye) as depicted by the DFT calculations.

Molecule	Optimized geometry	Total energy /a.u.	Dipole moment / Debye
Urea		-225.2607	4.7364
Ethylene glycol (EG)		-230.2119	3.1077

Urea-EG linear binary system		-455.5296	6.8136
Urea-EG 9-membered ring		-455.5211	7.786284

3.5. Comparison with other catalysts:

The electrocatalytic oxidation of EG using various catalysts has been investigated and the data are summarized in Table 2. Inspection of this table reveals that the proposed non-precious CuOx/Cu porous catalyst supports a significant oxidation current of EG compared with the Pt-based anodes. Furthermore, blending EG with urea showed a marked enhancement in the oxidation current of EG which is superior to the modification of Pt with other metal oxides, i.e., NiOx, MnOx or CoOx.

Table 2. Comparison of the electro-oxidation of EG at various metal oxide-based anodes in alkaline Medium (0.5 M NaOH).

Catalyst	[EG] / M	E_{onset} / mV	I_p / mA cm ⁻²	Ref.
Pt/GC	0.5	-460	9.0	21
NiOx/Pt/GC	0.5	-470	9.8	21
MnOx/Pt/GC	0.5	-580	15.5	25
CoOx/Pt/GC	0.5	-630	19.0	25
CuOx/Cu	0.1	410	118.4 ^(a)	This work
CuOx/Cu	0.1 + 0.02 M urea	260	157.5 ^(a)	This work

^(a) the peak current density is calculated on the basis of the geometric surface area of the CuOx/Cu catalyst.

4. CONCLUSION

In this paper, a microporous foam-like catalyst layer of copper/copper oxide was successfully prepared atop copper planar electrode using a dynamic hydrogen bubbles template (DHBT) technique. The as-prepared microporous CuO_x/Cu catalyst showed good electrocatalytic activity towards EG oxidation in alkaline medium. The oxidation peak current increases with EG concentration and the potential scan rate as well. Urea (as an additive) enhanced the electrocatalytic oxidation of EG to various extents depending on its molar ratio in the fuel blend. This is manifested by the increase of oxidation peak current (as depicted from CV), a favorable negative shift of the onset potential of the oxidation process (as depicted from LSV) and lowering of the charge transfer resistance (as depicted from EIS data). A proposed model assumed the formation of a linearly expanding binary chain of EG-urea and/or 9-membered ring structures between EG and urea (via H-bonding) in such a way that facilitated the electro-oxidation of EG. DFT calculations supported the proposed model as evident from the lower total energy together with the enhancement in the dipole moment upon the binding between EG and urea compared to the individual fuels.

References

1. T. Hofer, R. Madlener, *Energy Policy*, 139 (2020) 1112777.
2. S. E. Hosseini, M. A. Wahid, *Int. J. Energy Res.*, 44 (2020) 4110-4131.
3. I. M. Al-Akraa, A. M. Mohammad, M. S. El-Deab, B. E. El-Anadouli, *Int. J. Hydrogen Energy*, 40 (4) (2015) 1789 – 1794.
4. G. A. El-Nagar, A. M. Mohammad, M. S. El-Deab, T. Ohsaka, B. E. El-Anadouli, *J. Power Sources*, 265 (2014) 57 – 61.
5. M. I. Awad, M. S. El-Deab, T. Ohsaka, *J. Electrochem. Soc.*, 154 (8) (2007) B810-B816.
6. A. Kirubakaran, S. Jain, R. K. Nema, *Renew. Sust. Energy Rev.*, 13 (2009) 2430-2440.
7. J. M. Feliu, E. Herrero, *Handbook of Fuel Cells*, Wiley, New York (2003).
8. E. Antolini, E. R. Gonzalez, *J. Power Sources*, 195 (2010) 3431-3450.
9. B. B. Blizanac, P. N. Ross, N. M. Markovic, *Electrochim. Acta*, 52 (2007) 2264-2271.
10. K. Kordesch, V. Hacker, J. Gsellmann, M. Cifrain, G. Faleschini, P. Enzinger, R. Fankhauser, M. Ortner, M. Muhr, R. R. Aronson, *J. Power Sources*, 86 (2000) 152-165.
11. P. Gouerec, L. Poletto, J. Denizot, E. S.-Cortezon, J. H. Miners, *J. Power Sources*, 129 (2004) 193-204.
12. E. Gulzow, M. Schulze, U. Gerke, *J. Power Sources*, 156 (2006) 1-7.
13. B. Y. S. Lin, D. W. Kirk, S. J. Thorpe, *J. Power Sources*, 161 (2006) 474-483.
14. M. Duerr, S. Gair, A. Cruden, J. McDonald, *J. Power Sources*, 171 (2007) 1023-1032.
15. S. Wasmu, A. Kuver, *J. Electroanal. Chem.*, 461 (1999) 14-31.
16. E. Antolini, *J. Power Sources*, 170 (2007) 1-12.
17. E. Peled, V. Livshits, T. Duvdevani, *J. Power Sources*, 106 (2002) 245-248.
18. L. Xin, Z. Zhang, J. Qi, D. Chadderton, W. Li, *Appl. Cat. B Environ*, 125 (2012) 85-94.
19. A. M. Mohammad, G. H. El-Nowihy, M. H. Khalil, M. S. El-Deab, *J. Electrochem. Soc.*, 161 (2014) F1340-F1347.
20. Y. Zhu, S. Y. Ha, R. I. Masel, *J. Power Sources*, 130 (2004) 8-14.
21. G. H. El-Nowihy, A. M. Mohammad, M. M. Khalil, M. A. Sadek, M. S. El-Deab, *Int. J. Hydrogen Energy* 42 (2017) 5095-5104.
22. L. An, L. Zeng, T. S. Zhao, *Int. J. Hydrogen Energy*, 38 (2013) 10602-10606.

23. J. C. S.-Ruiz, *Advanced Biofuels: Using catalytic Routes for the Conversion of Biomass Platform Molecules*, CRC Press Inc., London, UK (2015).
24. L. An, T. S. Zhao, J. B. Xu, *Int. J. Hydrogen Energy*, 36 (2011) 13089-13095.
25. G. H. El-Nowihy, A. M. Mohammad, M. A. Sadek, M. H. Khalil, M. S. El-Deab, *J. Electrochem. Soc.*, 166 (6) (2019) F364-F376.
26. G. H. El-Nowihy, A. M. Mohammad, M. A. Sadek, M. H. Khalil, M. S. El-Deab, *Int. J. Electrochem. Sci.*, 12 (2017) 62-73.
27. P. A. Christensen, A. Hamnett, *J. Electroanal. Chem.* 260 (1989) 347-359.
28. K. matsouka, Y. Iriyama, T. Abe, M. Matsuoka, Z. Ogumi, *Electrochim. Acta*, 51 (2005) 1085-1090.
29. H. Kohlmuller, *J. Power Sources*, 1 (1976/1977) 249-256.
30. N. dalbay, F. Kadirgan, *Electrochim. Acta*, 36 (1991) 353-356.
31. F. Kadirgan, B. Beden, C. lamy, *J. Electroanal. Chem.*, 143 (1983) 135-152.
32. A. A. El-Shafie, H. M. Shabanah, M. N. H. Moussa, *J. Power Sources*, 46 (1993) 17-27.
33. M. Wala, W. Simka, *Molecules*, 26 (2021) 2144.
34. M. R. Rizk, M. G. Abd El-Moghny, G. A. El-Nagar, A. A. Mazhar, M. S. El-Deab, *ChemElectroChem.*, 7 (2020) 951-958.
35. D. Reyter, M. Odziemkowski, D. Belanger, L. Roue, *J. Electrochem. Soc.*, 154 (2007) K36-K44.
36. M. R. Rizk, M. G. A. El-Moghny, A. Mazhar, M. S. El-Deab, B. E. El-Anadouli, *Sust. Energy & Fuels*, 5 (2021) 986-994.
37. M. S. El-Deab, M. I. Awad, A. M. Saada, A. M. Attia, *Int. J. Electrochem. Sci.*, 16 (2021) 210549.
38. S. Trasatti, O. A. Petrii, *Pure & Appl. Chem.*, 63 (1991) 711-734.
39. M. S. El-Deab, M. M. Saleh, B. E. El-Anadouli, B. G. Ateya, *Int. J. Hydrogen Energy*, 21 (1996) 372-280.
40. L. Demarconnay, S. Brimaud, C. Coutanceau, J.-M. Leger, *J. Electroanal. Chem.*, 601 (2007) 169-180.
41. H. Wang, Z. Jusys, R. J. Behm, *Electrochim. Acta*, 54 (2009) 6484-6498.
42. T. Matsumoto, M. Sadakiyo, M. L. Ooi, S. Kitano, T. Yamamoto, S. Matsumura, K. Kato, T. Takeguchi, M. Yamauchi, *Sci. Rep.*, 4 (2014) 5620.
43. A. Di. Tocco, M. Granero, N. Robledo, A. Zon, N. Roberto, L. Mart, *Sens. Actuators B* 244 (2017) 949-957.
44. X. Niu, Y. Li, J. Tang, Y. Hu, H. Zhao, M. Lan, *Biosens. Bioelectron.*, 51 (2014) 22-28.
45. X. Niu, J. Pan, F. Qiu, X. Li, Y. Yan, L. Shi, *Talanta*, 161 (2016) 615-622.
46. S. K. Meher, G. R. Rao, *Nanoscale*, 5 (2013) 2089-2099.
47. G. A. El-Nagar, I. Derr, T. Kottakkat, C. Roth, *ECS Trans.* 80 (2017) 1013-1022.
48. I.-M. Hsing, X. Wang, Y.-J. Leng, *J. Electrochem. Soc.*, 149 (2002) A615-A621.
49. A. M. Mohammad, I. M. Al-Akraa, M. S. El-Deab, *Int. J. Hydrogen Energy*, 43 (2018) 139-149.
50. I. O. Baibars, M. G. A. El-Moghny, M. S. El-Deab, *Electrochim. Acta*, 410 (2022) 139992.
51. I. O. Baibars, M. G. A. El-Mogny, A. S. Mogoda, M. S. El-Deab, *J. Electrochem. Soc.*, 168 (2021) 054509.
52. M. S. El-Deab, G. A. El-Nagar, A. M. Mohammad, B. E. El-Anadouli, *J. Power Sources*, 286 (2015) 504-509.
53. G. A. El-Nagar, C. Roth, *Chem. Select*, 1 (2016) 5706-5711.
54. G. H. El-Nowihy, M. S. El-Deab, *J. Electrochem. Soc.*, 169 (2022) 046508.
55. G. H. El-Nowihy, M. S. El-Deab, *Renew. Energy*, 167 (2021) 830-840.
56. M. A. H. A. Tawab, M. G. A. El-Mogny, R. M. El Nashar, *Microchem. J.*, 158 (2020) 105180.